JOURNAL OF GEOPHYSICAL RESEARCH, VOL. 103, NO. D16, PAGES 19,649–19,661, AUGUST 27, 1998

Intercomparison of pulsed lidar data with flight level CW lidar data and modeled backscatter from measured aerosol microphysics near Japan and Hawaii

D. R. Cutten,[1] J. D. Spinhirne,[2] R. T. Menzies,[3] D. A. Bowdle,[1] V. Srivastava,[4]
R. F. Pueschel,[5] A. D. Clarke,[6] and J. Rothermel[7]

Abstract. Aerosol backscatter coefficient data were examined from two flights near Japan and Hawaii undertaken during NASA's Global Backscatter Experiment (GLOBE) in May-June 1990. During each of these two flights the aircraft traversed different altitudes within a region of the atmosphere defined by the same set of latitude and longitude coordinates. This provided an ideal opportunity to allow flight level focused continuous wave (CW) lidar backscatter measured at 9.11-μm wavelength and modeled aerosol backscatter from two aerosol optical counters to be compared with pulsed lidar aerosol backscatter data at 1.06- and 9.25-μm wavelengths. The best agreement between all sensors was found in the altitude region below 7 km, where backscatter values were moderately high at all three wavelengths. Above this altitude the pulsed lidar backscatter data at 1.06- and 9.25-μm wavelengths were higher than the flight level data obtained from the CW lidar or derived from the optical counters, suggesting sample volume effects were responsible for this. Aerosol microphysics analysis of data near Japan revealed a strong sea-salt aerosol plume extending upward from the marine boundary layer. On the basis of sample volume differences, it was found that large particles were of different composition compared with the small particles for low backscatter conditions.

1. Introduction

The study of tropospheric aerosols in remote regions has now become an important component for modeling cloud physics, radiative transfer, global transport, and climate forcing effects in the atmosphere [*Coakley and Cess*, 1985; *Albrecht*, 1989; *Charlson et al.*, 1992]. Often these investigations are done in the remote troposphere using moving platforms such as aircraft with sensors, which collect data on aerosol properties at aircraft flight level and at a distance from the aircraft. Sensors used in aerosol studies vary widely in the way the aerosol characteristics are obtained. In the case of aerosol backscatter coefficient measurements these data can be (1) measured directly with range-resolved pulsed lidars focused at infinity, (2) derived from aerosol microphysics at flight level, or (3) measured directly at aircraft level with a focused continuous wave (CW) lidar. Typically, pulsed lidars are unable to measure aerosol backscatter within ~1 km of the aircraft (due to nonoverlap of transmitted and received beams as well as optomechanical effects). This precludes directly comparing flight level derived aerosol backscatter with data measured by these lidars. Therefore one cannot compare the effects of lidar pulse length (i.e., sample volume) and time averaging with flight level backscatter data viewed horizontally from the same spatial region at the same time. The effect of sample volume is particularly important because of the large sampling volumes associated with pulsed lidars compared with sensors used to measure aerosol size distributions at flight level, i.e., lidars may more thoroughly sample sparsely distributed large particles.

The National Aeronautics and Space Administration (NASA) conducted the Global Backscatter Experiment (GLOBE II) in May-June 1990 [*Bowdle et al.*, 1991] over and around the remote Pacific Ocean. The centerpiece of GLOBE was an instrumented NASA DC-8 aircraft that operated in the troposphere. The aircraft carried a suite of sensors which allowed aerosol backscatter coefficients to be derived remotely using pulse lidars and at flight level using CW lidar. Several of the flights were arranged such that the aircraft traversed the same region of atmosphere which had shortly beforehand been remotely sampled by two pulsed lidar systems. In this paper the results of aerosol backscatter coefficient intercomparisons at several wavelengths are presented, using data from five different sensors. Explanations are provided for aerosol backscatter coefficient variations in terms of instrument performance, aerosol microphysics, and composition prevailing at the time.

[1]Earth System Science Laboratory, Global Hydrology and Climate Center, University of Alabama in Huntsville.

[2]NASA Goddard Space Flight Center, Greenbelt, Maryland.

[3]NASA Jet Propulsion Laboratory, Pasadena, California.

[4]Universities Space Research Association, Global Hydrology and Climate Center, Huntsville, Alabama.

[5]NASA Ames Research Center, Moffett Field, California.

[6]School of Oceanography, University of Hawaii, Honolulu.

[7]Global Hydrology and Climate Center, NASA Marshall Space Flight Center, Huntsville, Alabama.

Paper number 98JD01155.
0148-0227/98/98JD-01155$09.00

2. Flight Details

Aircraft flight details and meteorological conditions are presented for two flights which took place near Japan and Hawaii as part of the GLOBE II Pacific Ocean survey mission using the NASA DC-8 aircraft.

2.1. Japan Flight

This flight (number 13 in the GLOBE II flight series) took place on June 3, 1990, from 0108 to 0808 UTC, over the Pacific Ocean, SE of Tokyo, Japan. The data reported here were obtained from 0240 to 0545 UTC for all sensors. This portion of the flight basically consisted of a series of ~280-km level flight legs from NW to SE at 11.5, 9.8, 6.5, and 3.2 km between (26.10° N, 146.70° E) and (23.74° N, 148.66° E). Each level flight leg (see Figure 1a) was followed by a gradual descent in the opposite direction to the starting point of the next level flight leg. The slow descents provided detailed vertical profiles from the flight level instruments, for comparison with the pulsed lidar profiles obtained remotely along the same flight track. An exception to this pattern was the rapid descent from 11.5 km where the DC-8 reached the 9.8-km level well before the NW end point of the intercomparison ground track. In this case the aircraft retraced a large portion of this flight level twice but in opposite directions.

Meteorological conditions during this flight featured a 40 m s^{-1} westerly jet above 8-km altitude near Tokyo. The jet gradually weakened as the aircraft progressed southeastward during the first 1.5 hours of the flight. Considerable cloudiness was found throughout the troposphere, especially near Japan, associated with a cold front trailing from a midlatitude cyclone northeast of Japan. Additional cyclogenesis was evident southwest of Kyushu in response to the approach of a new synoptic wave moving out of Mongolia. Between 0230 and 0300 UTC, as the aircraft approached its farthest point from Tokyo, it encountered weak easterlies near 11-km altitude, indicating the aircraft's traversal of the core of the belt of subtropical anticyclones south of Japan. The aircraft then executed its first U-turn and began its series of flight legs at ever decreasing altitudes. During these descending flight legs, winds at flight level shifted to the northwest quadrant, at speeds of 10 m s^{-1} or less (see Figure 2) and remained from that quadrant until the aircraft ultimately regained altitude and headed back toward Tokyo. At no time did the aircraft encounter clouds during the maneuver. However, a complex pattern of haze layers and sudden changes in ambient dewpoint at some flight levels during the descending flight legs were observed. Examining Figure 2a shows that the wind direction during the highest stepped descents (9.8 and 11.5 km) was mostly at an angle of 50° to the flight track (these angles are indicated by the two dashed lines in the figure). With wind speeds between 5 and 10 m s^{-1} the aircraft exhaust would be sufficiently removed from the area when the lidar remotely sensed the higher flight levels from below. Contamination at the higher altitudes would be of concern because of low aerosol backscatter generally prevailing.

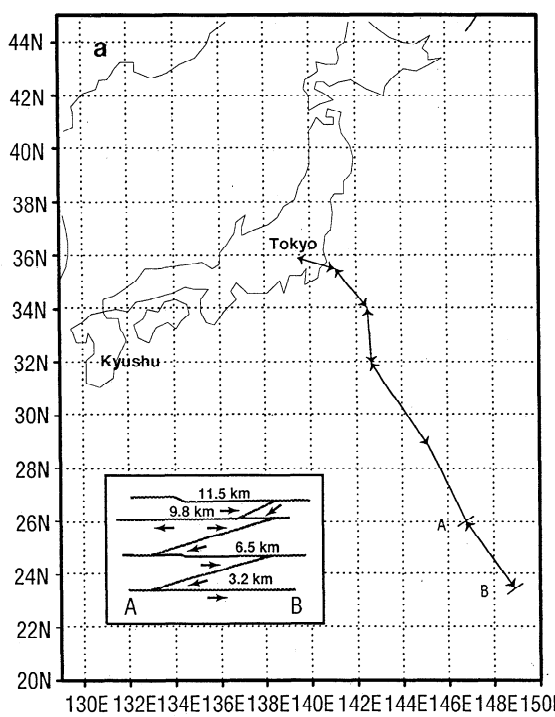

Figure 1. Flight tracks near (a) Japan on June 3, 1990, and (b) big island of Hawaii on May 18-19, 1990. The flight southeast of Tokyo consisted of four stacked flight levels between points A and B at the altitudes indicated in the insert, while the Hawaii flight was composed of four closed loops (at constant altitudes indicated).

2.2. Hawaii Flight

This flight (number 5 in the GLOBE II flight series) took place around the big island of Hawaii on May 18-19, 1990, from 2114 to 0142 UTC. Figure 1b shows a three-dimensional (3-D) view of the flight track above the island of Hawaii. It consisted, in part, of four complete loops near the coast of the island at 4.0-, 6.4-, 9.4-, and 12.5-km heights, maintaining the same course position for each loop and rapidly climbing to the next level at the NW corner of the island.

Meteorological conditions at the time of this flight were influenced by the recent passage of a sharp middle and upper tropospheric trough, the trailing portions of which were just northeast of the islands, and by a convective cluster along the Intertropical Convergence Zone (ITCZ) south of the islands. Lower tropospheric winds were generally from the northeast at 10 m s^{-1} backing to the north at roughly 20 m s^{-1} in the middle troposphere. Near 12-km altitude, a westerly jet having speeds from 40-50 m s^{-1} prevailed. The atmosphere was moist below 700 hPa, and surface dewpoints near 20°C sustained scattered convective showers topped by layers of detrained altocumulus. A thermal inversion was present near 700 hPa, and substantial amounts of haze were trapped below this layer. Above 700 hPa, the air was much drier, with only patches of cirrus near the islands. A region of more widespread cirrus detrained from the ITCZ was visible to the south.

3. Measurements

The lidar instrumentation consisted of three lidar systems operating at six wavelengths. Pulsed lidar systems were provided by NASA Jet Propulsion Laboratory (JPL) operating at a single wavelength of 9.25 μm [*Menzies and Tratt*, 1994] and by NASA Goddard Space Flight Center (GSFC) operating at 0.53-, 1.06- and 1.54-μm wavelengths [*Spinhirne et al.*, 1997]. Two focused CW Doppler lidar systems operating at

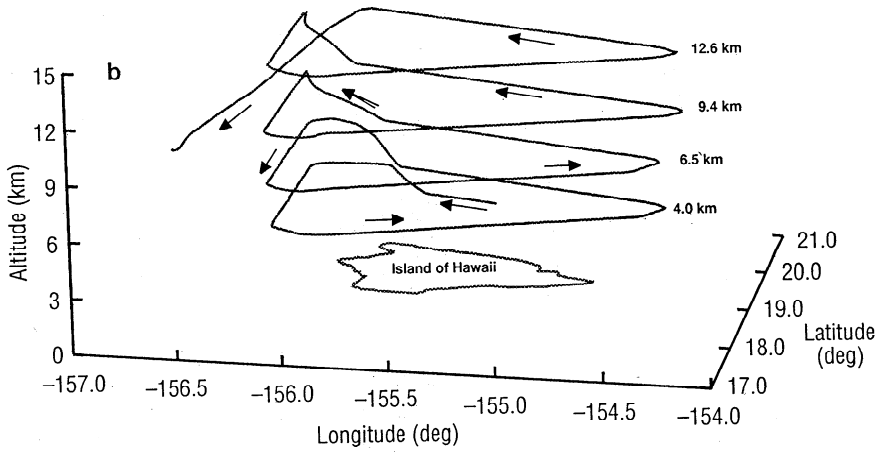

Figure 1. (continued)

9.11- and 10.59-μm wavelengths were provided by NASA Marshall Space Flight Center (MSFC) [*Rothermel et al.*, 1996]. All three lidars were calibrated to measure absolute aerosol backscatter coefficient (β, m^{-1} sr^{-1}) as described in the reference to each system listed above.

The aerosol size distribution at flight level was measured using two different optical particle counters (OPC). A wing-pod-mounted forward scattering spectrometer probe (FSSP), model 300, from NASA Ames Research Center (ARC) covered the diameter range 0.35-20 μm with 10-s temporal resolution [*Pueschel et al.*, 1994]. The University of Hawaii laser optical particle counter (LOPC) covered the size range 0.16- to 7.0-μm diameter using sampling times that were of the order of several minutes [*Clarke*, 1991, 1993]. A detailed summary of these sensors and their sampling characteristics has been given elsewhere [*Cutten et al.*, 1996]. In addition, an ultrafine condensation nuclei (UCN) counter measured nuclei between 3- and 15-nm diameter, while a second counter measured condensation nuclei (CN) above 15-nm diameter [*Clarke*, 1993]. The latter counter also measured nuclei in ambient and heated aerosol to provide data on the CN refractory component. Table 1 lists the uncertainty in β measured by each of the lidars and the uncertainty in the OPC-measured aerosol size distributions. The final uncertainty in the OPC-modeled β will be affected by uncertainties in the modeled aerosol composition, which are difficult to quantify. However, data indicate that the LOPC-modeled β uncertainty is of similar magnitude as the CW lidar β.

3.1. Size Distribution Data

The FSSP size distribution data were processed as described by *Cutten et al.* [1996]. This consisted initially of resizing the FSSP sample bins using LOPC-modeled aerosol refractive index data at 0.55-μm wavelength. The 10-s $dn/d\log D_p$ data were then averaged over 100 s and fitted to single-mode lognormal curves. The fitting process minimizes the effects of poor count statistics in the large particle regime. The FSSP underestimates bin counts in the 0.8- to 3-μm diameter range because of inadequate sampling; this size range dominates infrared β [*Srivastava et al.*, 1992]. Consequently, it has been found [*Cutten et al.*, 1996] that FSSP-modeled β less than 10^{-10} m^{-1} sr^{-1} in the infrared wavelength region (9-11 μm) can be as much as a factor of 3 smaller than measured data even with the curve fitting applied.

FSSP-measured size distributions were used to calculate β from Lorentz-Mie theory and LOPC-modeled aerosol refractive index data. The refractive index data were derived from inferred mixtures of sulfuric acid, ammonium sulfate, and dust using volumetric mixing rules. A growth correction was included due to relative humidity differences between ambient and LOPC sampling volume. Calculations for β were done at 1.06- and 9.11-μm wavelengths. Since the differences in refractive index of acid sulfate at 9.11- and 9.25-μm wavelengths are very small, measured and modeled β at 9.11-μm wavelength can be directly compared with measured β at 9.25-μm wavelength. Here β was also modeled from LOPC size distribution data based on aerosol mixture models described by *Srivastava et al.* [1997] that were most suitable for different aerosol loading conditions. Using the differences between the thermally segregated LOPC size distribution, volumes of different compositions were inferred. In cases of midtroposphere clean aerosol loading conditions, the mixed phase sulfate model was used to calculate refractive indexes of each LOPC size bin. For higher loading cases with a dominant dust component, a composite model was used for estimating the refractive index of the aerosols. These were used in Lorentz-Mie calculations to get β for different wavelengths.

3.2. Lidar data

JPL and GSFC pulsed lidar β data were processed in two ways. Data were extracted from those portions of nadir or zenith profiles within 0.5-km altitude of any selected flight level. These backscatter data were then averaged, either in altitude for time series along each leg or in time and altitude for a composite on each leg. These averaged data could then be compared directly with modeled or measured β at flight level, either in a time series format or in an altitude versus β format. The second way of processing the data involved temporally averaging the measured profiles over time during each constant-altitude leg from four flight levels for the Japan flight and from two flight levels for the Hawaii flight. These profiles were used to evaluate the range correction profile for each pulsed lidar. They also provided an indication of any temporal variability in the aerosol field during each intercomparison

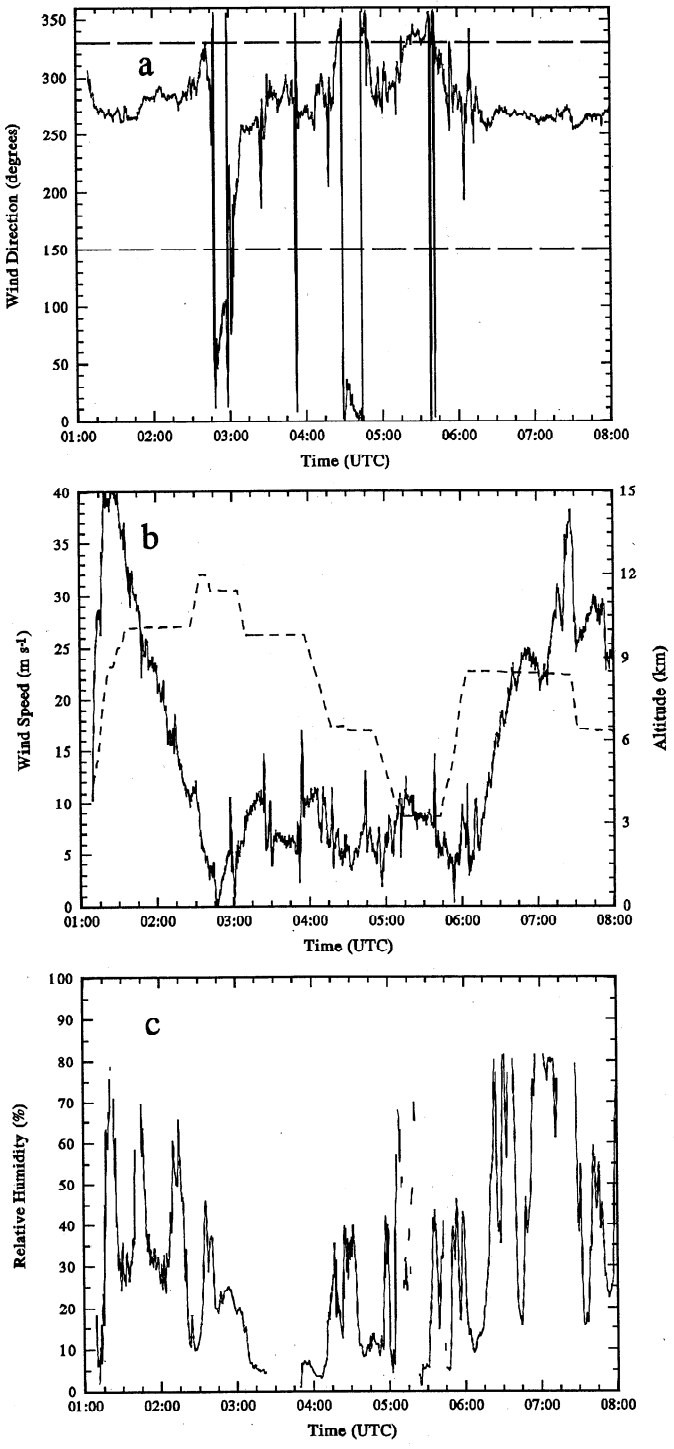

Figure 2. Time series of (a) wind direction, (b) wind speed, and (c) relative humidity along the flight track near Japan (Figure 1a). The dashed lines in Figure 2a show track angles for the intercomparison period. Dashed line in Figure 2b is aircraft altitude.

experiment. Lidar β profiles were not always available at each level in the two case studies. This was because the lidars were at times pointing in the zenith and not nadir direction when the aircraft was at the higher altitudes, problems with the instrumentation, or backscatter from intervening clouds. Averaging processes excluded any GSFC or JPL β data contaminated by cloud returns.

In the case of the 9.11- and 10.59-μm β data from the MSFC CW Doppler lidar, all 3-s β data falling within the FSSP-modeled β 100-s averaging period were averaged to provide coregistered data. For the time series plots, a 300-s "boxcar" running average was applied to both sets of data.

4. Intercomparison of OPC Modeled and Lidar β

This section will examine and evaluate the intercomparison of measured and modeled β data from pulsed lidars and in situ sensors for flights near Japan (section 4.1) and Hawaii (section 4.2).

4.1. Japan Flight

Before beginning the β intercomparison discussion, the dominant aerosol feature observed in this flight will be presented. Plate 1 shows a time-altitude false color cross section of logarithm of $\beta_{1.06}$ for the whole of Japan flight (subsequently referred to as 1.06-μm colorized β plot). The near-continuous, high-resolution (60 s) vertical profiles making up this image clearly show an aerosol plume extending vertically from the marine boundary layer (MBL). This feature is clearly reproduced when the aircraft repeated its track at different altitudes. The corresponding 9.25-μm colorized β image (not shown) did not show this feature as clearly because (1) most of the backscatter is from larger particles, and (2) a longer profile integration time (100 s) was used along with a 20-s gap between each profile.

4.1.1. 1.06 μm. A time series plot of measured and modeled $\beta_{1.06}$ for the two lowest altitudes is shown in Figure 3. At both altitudes, the time series for each instrument shows transects of the plume denoted by regions A, B, and D in Plate 1. The plume provided a prominent intercomparison target, with β values at each altitude ranging over nearly an order of magnitude along each ~280-km transect. The highest values, ~4×10^{-8} m^{-1} sr^{-1}, occur in the plume peak at 3.2-km altitude. The lowest values, ~7×10^{-9} m^{-1} sr^{-1}, occur in the plume fringes at 6.5-km altitude. In all cases, $\beta_{1.06}$ values are well above the nominal detection threshold of the GSFC lidar and the count-limited detection thresholds of the FSSP and LOPC for modeled $\beta_{1.06}$ [*Cutten et al.*, 1996].

At both altitudes, plume transects for each instrument show well-defined peak and fringe features. Details vary with altitude, instrument, and sample period. In particular, as the flight progressed, the peak value occurred later in the transect, ~4.8 min (66 km) at 6.5-km altitude from 0240 to 0532 UTC and ~2.4 min (33 km) at 3.2-km altitude from 0240 to 0337 UTC. (DC-8 true air speed was 230 m s^{-1}.) These displacements are consistent with plume advection by the mean along-track wind at each altitude (50 and 34 km at 6.5- and 3.2-km altitude, respectively). Subsequent discussions of the intercomparison results at these two altitudes will assume that plume properties at each altitude did not change with the movement of the plume. This assumption allows comparisons of the magnitudes and temporal trends in the corresponding time series.

The GSFC lidar data show excellent agreement (within 5%) in both magnitude and trend for almost all segments of the successive time series at both altitudes. The largest discrepancies occur in the last run, where the first few minutes show higher β

Table 1. Uncertainties for Lidar and Optical Particle Counter Data

Instrument	Wavelength, μm	Sample Volume, m^3	Threshold β Level, m^{-1} sr^{-1}	Δβ, m^{-1} sr^{-1}	Δn, cm^{-3}
GSFC pulsed lidar	0.53	4×10^5	5×10^{-9}	$\pm1\times10^{-8}$	–
GSFC pulsed lidar	1.06	4×10^5	1×10^{-9}	$\pm1\times10^{-9}$	–
MSFC CW lidar	9.11	6×10^2	6×10^{-12}	$\pm2.4\times10^{-12}$ *	–
JPL pulsed lidar	9.25	6×10^4	1×10^{-11}	$\pm2\times10^{-11}$	–
			at 2 km from aircraft		
MSFC CW lidar	10.59	6×10^2	2×10^{-11}	$\pm7.2\times10^{-12}$ *	–
FSSP	–	1×10^{-3}	–	–	<±30% †
LOPC	–	1.7×10^{-3}	–	–	<±20%

* Note that the two CW lidar uncertainty values given in Table 2 by *Cutten et al.* [1996] were incorrect and should be replaced with these values.

†FSSP uncertainty based on count statistics for size bins >0.8-μm diameter.

by ~50% and the last few minutes show lower β by ~30% than the earlier runs. Both time series for the FSSP-modeled $\beta_{1.06}$ match the trends in the corresponding GSFC time series (typically within 20%). However, at both altitudes the FSSP data are systematically lower than the GSFC data (a factor of 2 at 3.2 km and a factor of 4 at 6.5 km), which is probably due to different sampling volumes of the sensors. By contrast, the peak and minimum values in the LOPC $\beta_{1.06}$ time series show good agreement (within 10%) with the corresponding extrema in the GSFC data but significantly more disagreement (20-100%) in details of the temporal trends. In particular, LOPC peak values typically occur ~5-7 min after FSSP peak values in the same time series and therefore ~5-7 min after the corresponding GSFC peak values.

The plume properties at 3.2 km and 6.5 km were essentially invariant throughout the intercomparison period. They show internal consistency in the GSFC $\beta_{1.06}$ profiles for several independent ranges and beam orientations (8.2-km nadir versus 6.6-km nadir for the 3.2-km data and 5-km nadir versus 3.3-km nadir versus 3.3-km zenith for the 6.5-km data). They also confirm the inherent reliability of $\beta_{1.06}$ modeling using aerosol microphysical measurements from the LOPC, after standard corrections for sampling effects. Since the FSSP and GSFC trends showed good agreement, the discrepancies between the LOPC and GSFC trends can be attributed to long LOPC integration times (~10 min, versus 100 s for the FSSP and 60 s for GSFC data) in the presence of strong systematic aerosol gradients.

The time-averaged GSFC aerosol β profiles (Figure 4) reveal very good consistency among the individual profiles considering that they were measured several hours apart, with the biggest deviations occurring only at 4.7, 7, and 9 km. Therefore aerosol temporal variability over the selected measurement periods can be considered to be minimal for the 1.06-μm wavelength throughout the troposphere. In fact, the residual discrepancies are due primarily to sampling successively different portions of the same features as those features drifted across the intercomparison region. The overall trend in all of the profiles is to a lower β up to 10 km, which then remains constant at around 1 x 10^{-8} m^{-1} sr^{-1} up to 15 km. Figure 4 also shows data for the GSFC lidar and FSSP and LOPC sensors in a different format at the four intercomparison altitudes. Here the time averaged β and corresponding upper and lower limits for each set of GSFC, FSSP, and LOPC data are plotted to indicate how the averaged data compare: Data used to compute the GSFC average β are the ±0.5-km data from all time periods available at that altitude. For the lower two altitudes the average and range for the GSFC, LOPC, and FSSP data all agree within a factor of 2-3. As noted previously, the GSFC and LOPC data show the best agreement, with the FSSP consistently showing lower values. At the two higher altitudes the agreement is generally poorer, with the FSSP data again showing the largest difference. The LOPC data are in good agreement with the GSFC lidar data at 9.8-km altitude, while at the 11.5-km altitude, the LOPC data are also lower. At these altitudes a predominant fraction of the β in these cleaner regions was found to arise from a large number of smaller particles (<0.5-μm diameter) and an absence of larger particles. Hence, since the FSSP samples particles in a very restricted size range, the FSSP-modeled β will be underestimated.

4.1.2. 9.25 μm. The JPL lidar β data obtained at constant altitude during the Japan flight are shown as a time series in Figure 5, again at the same two flight altitudes as for the 1.06-μm data (Figure 3). Along with these data are also shown the 100-s FSSP-modeled, LOPC-modeled, and 100-s CW lidar measured β, all at flight level. Figure 6 shows time-averaged JPL profiles for each of the three time intervals examined, along with a set of averaged data from each sensor. At the two lower altitudes (3.2 and 6.5 km; Figure 6), mean β values agree to within a factor of ~3 for all four flight level sensors. However, the spread for the CW lidar data is quite large at the 6.5-km level, as well as for the LOPC data at 3.2 km. At 9.8-km altitude (not shown in Figure 5) the mean values differ by over a decade. However, the CW β lidar data and FSSP- and LOPC-modeled β agree to within a factor of ~1.5 at 11.5-km level. The first 3 km of the 0518-0538 UTC profile up to 7 km has a similar shape to the corresponding portion of the 0424-0442 UTC profile although displaced to higher β values. The profile was truncated at 9 km because of excess noise between 9 and

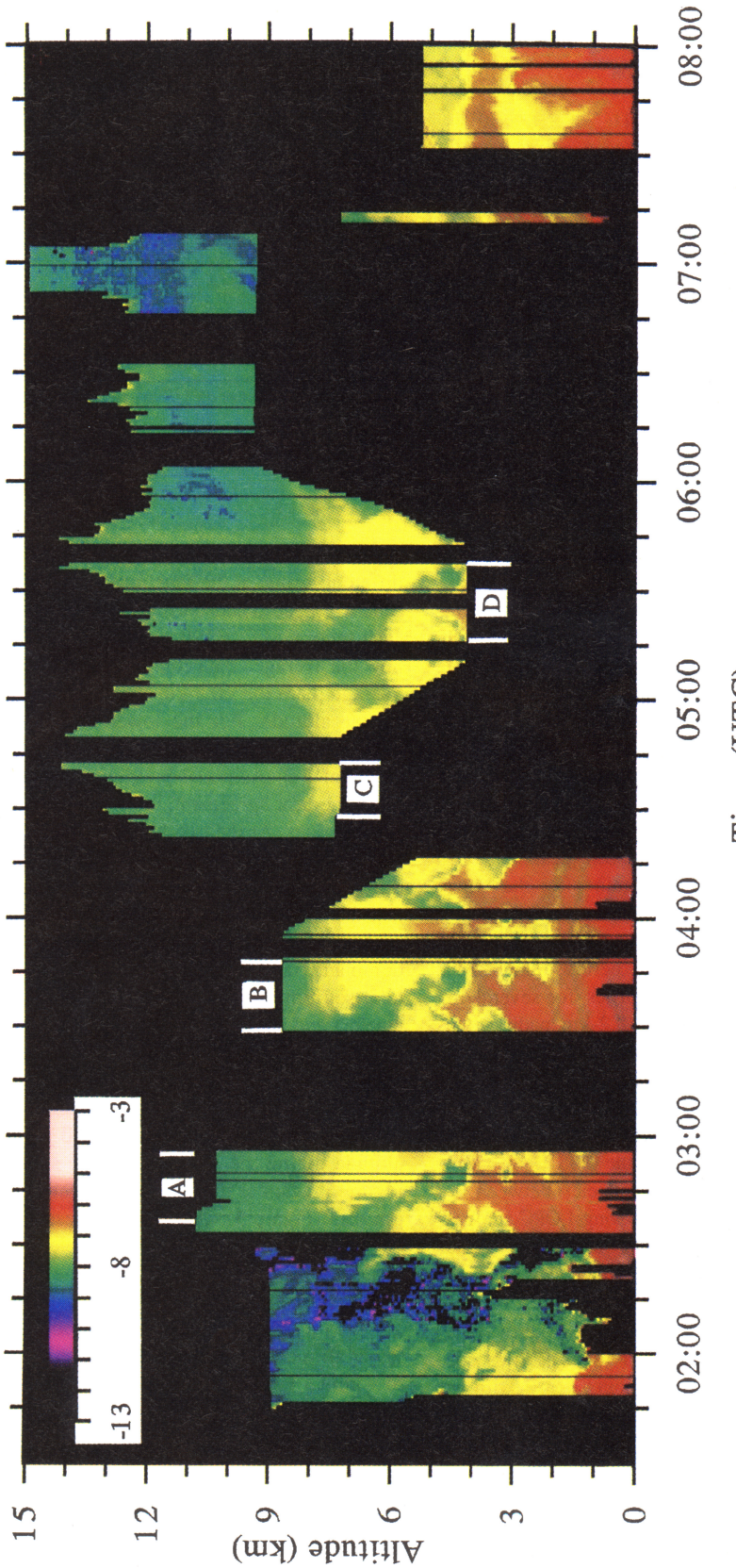

Plate 1. False-color cross section of logarithm of 1.06-μm aerosol backscatter near Japan on June 3, 1990. Regions marked A, B, C, and D are periods used for sensor intercomparison.

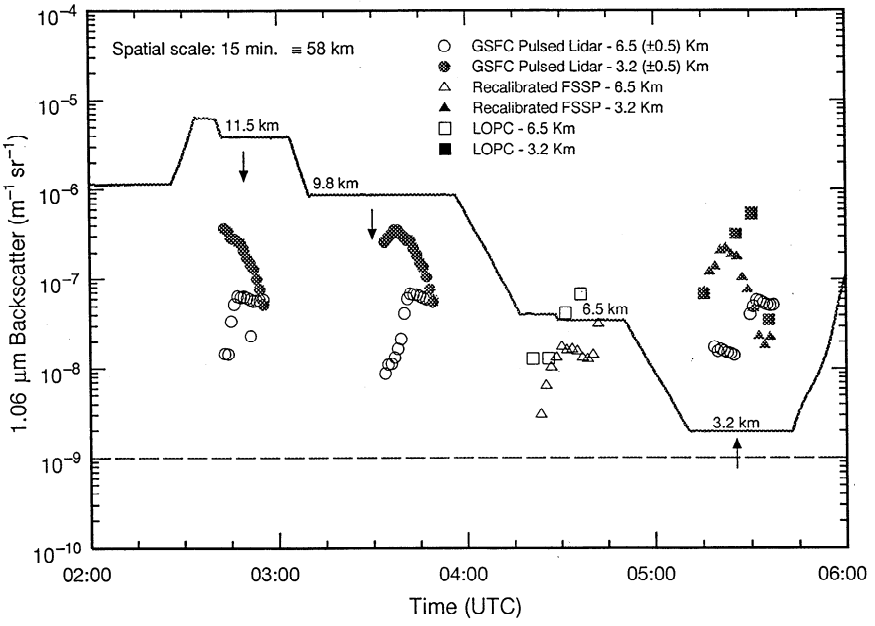

Figure 3. Time series plot of measured and modeled 1.06-μm aerosol backscatter coefficient β for selected periods from the Japan flight on June 3, 1990. Lidar data are averaged over ±0.5 km of the two flight altitudes studied. The β data modeled from the forward scattering spectrometer probe (FSSP) and laser optical particle counter (LOPC) flight level sensors are superimposed. Dashed horizontal line at 1 x 10^{-9} m^{-1} sr^{-1} represents the Goddard Space Flight Center (GSFC) lidar sensitivity level. Remaining line is flight altitude; arrows represent GSFC lidar pointing direction.

11.5 km and because of cirrus above this region. The two nadir profiles below 3 km are similar, particularly across the strong cloud layer at about 0.9 km.

The intercomparison results below 6.5 km for the two wavelength regions show remarkably good overall agreement, within 5-10%, where aerosol temporal variability was shown to be minimal. The precision of this comparison is far better than was possible during the transit flights, where modeled β at flight level could only be compared with measured β within 1-2 km altitude from the aircraft [*Cutten et al.*, 1996]. In fact, the only anomalies in the comparisons discussed so far for $\beta_{1.06}$ data are the constant discrepancy in the FSSP $\beta_{1.06}$ data at a given altitude and the change in magnitude of the discrepancy

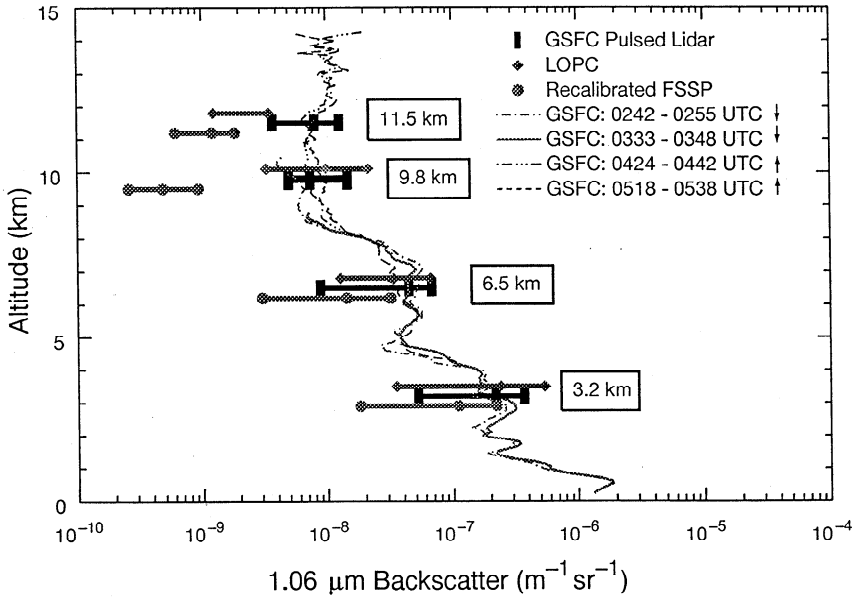

Figure 4. Backscatter profiles near Japan based on 1.06-μm GSFC profiles for several time periods and beam orientations (solid, dashed, and dash-dotted lines), GSFC data averaged over ±0.5 km of the flight altitudes listed (vertical bars), and aerosol backscatter modeled at flight level from FSSP (circles) and LOPC (diamonds) sensors. Horizontal bars and associated symbols show range of data and averages for each sensor. Bars at each altitude have been slightly displaced vertically for clarity.

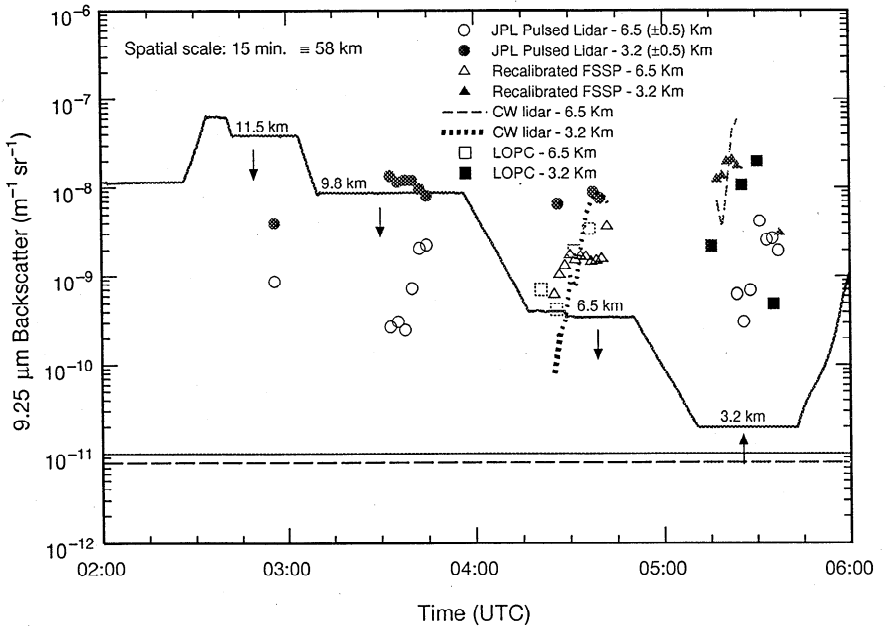

Figure 5. Time series of measured and modeled 9.25-μm aerosol backscatter coefficient for selected periods from Japan flight on June 3, 1990. Jet Propulsion Laboratory (JPL) data are averaged over ±0.5 km of two flight altitudes studied. Plot includes flight level aerosol backscatter (β) data modeled from the FSSP (triangles) and LOPC (squares) sensors, and measured β using 9.1-μm CW Doppler lidar (dotted and dashed lines). Solid and dashed horizontal lines at 1×10^{-11} and 6×10^{-12} m^{-1} sr^{-1} represent sensitivity levels for JPL (near aircraft) and CW lidars, respectively. Remaining solid line is flight altitude; arrows represent JPL lidar pointing directions.

with altitude. In cleaner regions of the troposphere (where $\beta_{1.06} < 10^{-8}$ m^{-1} sr^{-1}), smaller particles (<0.5 μm) contribute most to β [*Clarke*, 1993]. Since the FSSP is unable to sample these small particles adequately, this will lead to a considerable underestimate of $\beta_{1.06}$, providing an explanation for the FSSP discrepancy seen at higher altitudes. Both show variability in modeled β OPCs in the 9.25-μm region, particularly at 9.8-km level, which may be the result of small sampling volumes. However, the mean FSSP-modeled and CW lidar β (the only lidar data available at the higher altitudes) are similar. This may be due to an absence of a significant number of large particles (mentioned above), resulting in most of the infrared β originating from particles less than 1-μm diameter. Under these conditions, modeled β based on FSSP counting statistics will not be greatly affected by the problem of the FSSP undersampling the large particles [*Cutten et al.*, 1996], but instead will

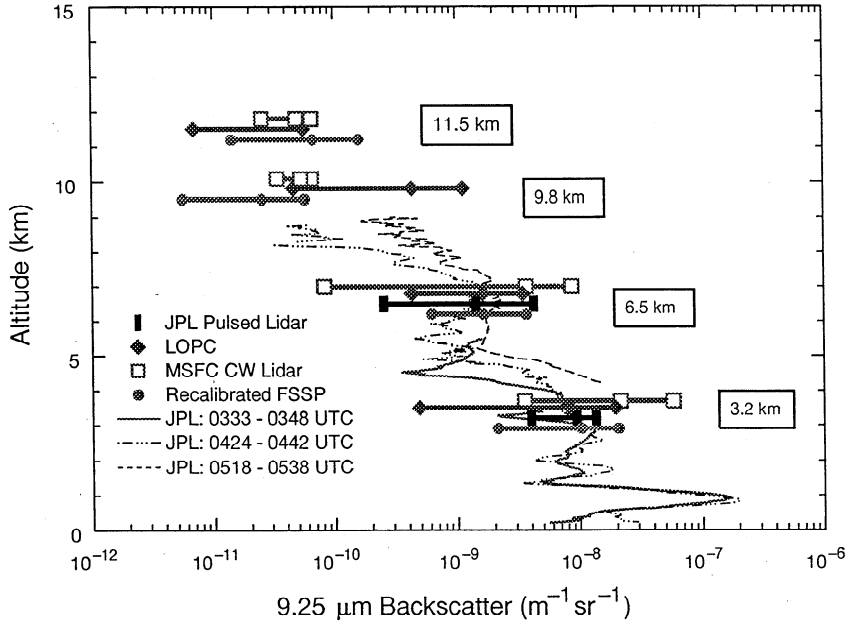

Figure 6. Same as Figure 4, but for 9.25-μm wavelength; includes β measured by 9.11-μm CW Doppler lidar (squares). Note no JPL profile for 0242-0255 UTC.

be dominated by counting statistics in the 0.35- to 1.0-μm diameter range.

4.2. Hawaii Flight

For the second β intercomparison from remote and in situ sensors, complete sets of lidar β data were used for the lower two levels (6.5 and 3.2 km) around the big island of Hawaii. At the 9.4- and 12.5-km flight levels the GSFC lidar was pointed in the zenith direction, while the JPL lidar data contained numerous dropouts owing to weak backscatter.

4.2.1. 1.06 μm. Figure 7 shows $\beta_{1.06}$ data as a time series plot for two altitudes. The FSSP and GSFC lidar at 4-km altitude compare well, with the spread of data from each sensor confined to less than an order of magnitude. Here the β was dominated by particles above 1-μm diameter where the FSSP had moderate counts. On the other hand, LOPC-modeled $\beta_{1.06}$ are about 50% higher.

At the 6.5-km altitude the FSSP-modeled $\beta_{1.06}$ show large scatter. An examination of the false color time series plot of the FSSP size distribution (not shown) indicated that the particle numbers within the size range 1.2- to 3-μm diameter fluctuated over this period. Particle numbers in this size range showed two strong peaks (at 2324 and 2336 UTC) where counts were observed in all size bins. The suggestion is that a well-defined aerosol layer was encountered with orientation N-S, since these times correspond to transects of the same longitude. (Winds at this altitude were from the north at ~15 m s^{-1}.) The GSFC data for 2350-0000 UTC are a factor of ~2.5 above the FSSP-modeled $\beta_{1.06}$ for the leg at 2300-2312 UTC owing to (1) the lower cutoff limit of the FSSP sensor and (2) the GSFC lidar sample volume probably detecting more β from particles larger than 1-μm diameter because of spatial inhomogeneities associated with moderately low β. Because of its long sampling times, the LOPC sensor tended to average out these inhomogeneities. However, the GSFC data all lie above the mean FSSP-modeled $\beta_{1.06}$, which may be due to the choice of aerosol components since the same composition was assumed as for the 4-km level. Figure 8 shows two GSFC lidar nadir profiles measured from 6.5- and 9.5-km altitude levels at 2300-2345 and 2350-0000 UTC, respectively, and averaged over the time periods shown in the figure. Again the agreement between the two profiles is very good. This $\beta_{1.06}$ profile comparison, which occurred early in the GLOBE II mission and the Japan profile comparison from the latter part of the mission, indicates the GSFC lidar was performing consistently during the GLOBE II experiment.

4.2.2. 9.25 μm. Figure 9 shows a time series plot of JPL lidar β data and β from each of the flight level sensors at two altitudes (4 and 6.5 km). Agreement to within a factor of ~3 or less exists at 4 km among the CW lidar and FSSP and LOPC sensors. However, the JPL lidar β data were nearly an order of magnitude lower around 2340 UTC and over the period 0035-0120 UTC. At 6.5 km the CW lidar and FSSP and LOPC sensors all show large fluctuations in β. This arose from transecting a N-S aerosol plume at 154°W on two sides of the closed flight path (see the 1.06-μm discussion above). The FSSP sensor and CW lidar fluctuations are to some degree correlated, although the amplitudes of the CW lidar fluctuations are smaller by over an order of magnitude. The LOPC sensor exhibits smaller fluctuations but at higher levels. The JPL β measured 1.5 hours later at this altitude exhibits larger fluctuations compared with 4.0 km but much smaller compared with the FSSP.

The β intercomparison between the lidar and OPC sensors in this flight did not show as good an agreement for the flight near Japan. More β fluctuations were evident partly due to aerosol temporal variations at a given altitude, particularly at 6.5 km. However, the best agreement seen at 4 km (between CW lidar, and both OPCs) supports the previous conclusion in section 4.1.1 that the best agreement between lidars and OPCs is for moderate β values (>10^{-9} m^{-1} sr^{-1})

To summarize, comparisons of measured and modeled β during the two flights showed differing results for the two wave-

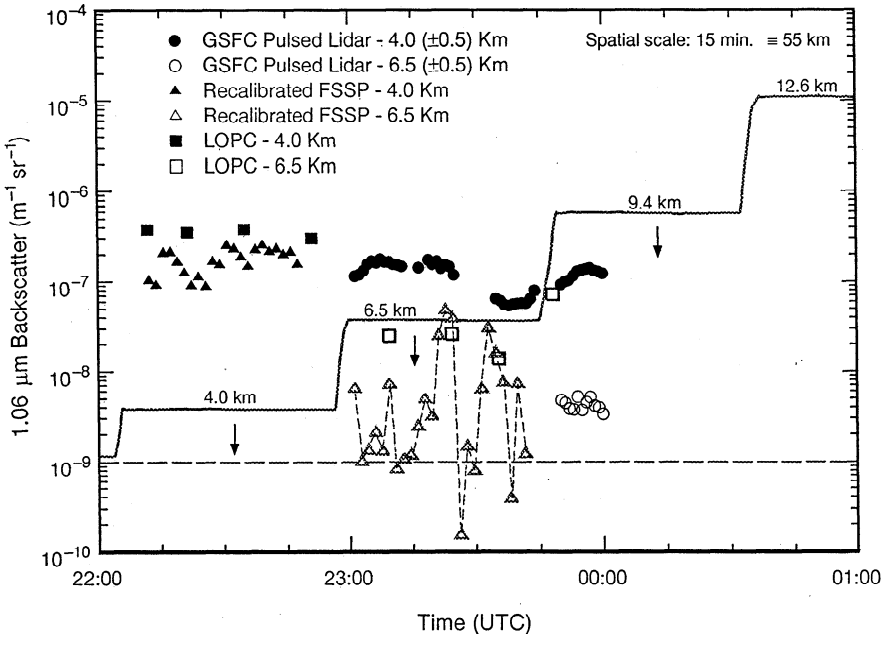

Figure 7. Same as Figure 3 for Hawaii flight on May 18-19, 1990.

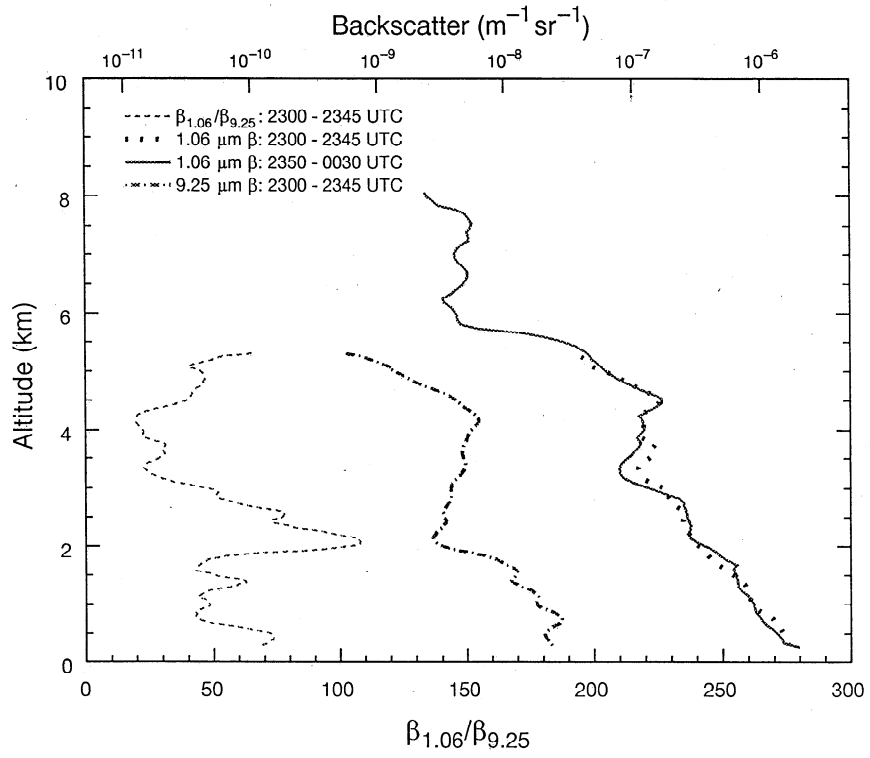

Figure 8. Two 1.06- and one 9.25-μm aerosol backscatter profiles averaged over time periods during Hawaii flight and $\beta_{1.06}/\beta_{9.25}$ profile averaged over 2305-2345 UTC.

lengths. The best agreement at 1.06-μm wavelength occurred when $\beta_{1.06}$ values were $>10^{-8}$ m^{-1} sr^{-1}. However, the smaller FSSP-modeled $\beta_{1.06}$ in this β range is partially the result of the lower diameter cutoff (0.35 μm), which will cause $\beta_{1.06}$ to be underestimated by as much as 20%. In tropospheric regions where $\beta_{1.06}$ $<10^{-8}$ m^{-1} sr^{-1}, it appears the β was dominated by particles near or below the FSSP lower cutoff diameter. Furthermore, both OPC sampling volumes are much smaller than the GSFC lidar sampling volume, which in the presence of aerosol inhomogeneity can lead to incomplete sampling and consequently more scatter in modeled $\beta_{1.06}$. The calibrated GSFC lidar, which measured β from particles over a large size range, is less likely to be affected by small spatial inhomogeneities and will likely show less $\beta_{1.06}$ variation. Agreement between measured and modeled β at 9.11- and 9.25-μm wavelengths was best for β values $>4x10^{-10}$ m^{-1} sr^{-1} which gen-

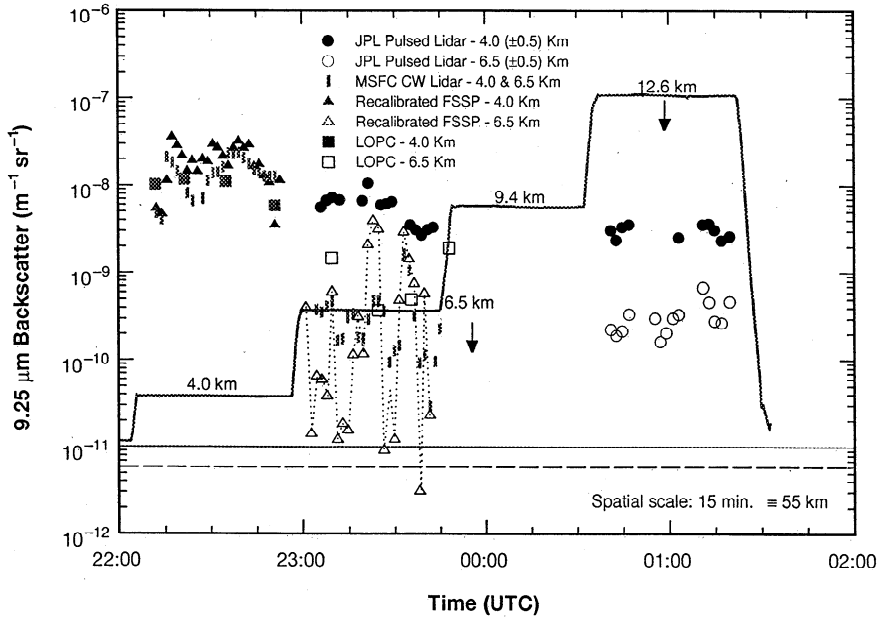

Figure 9. Same as Figure 5 but for Hawaii flight on May 18-19, 1990.

erally occurred below 7-km altitude at both measurement locations. For β values $<10^{-10}$ m^{-1} sr^{-1}, agreement was more difficult to ascertain because of higher aerosol variability.

5. Aerosol Composition

This section will examine the aerosol composition prevailing at the two locations using measured β, β ratio, LOPC-modeled β, and CN data. A list of β ratios for several different aerosol compositions and wavelengths is given in Table 2, taken from theoretical calculations based on single mode lognormal size distributions [*Srivastava et al.*, 1992]. Here $\beta_{9.11}/\beta_{10.59}$ provides data on particle composition [*Srivastava et al.*, 1995]. In low β regimes, $\beta_{9.11}/\beta_{10.59}$ near 10 is due to an ammoniated aerosol comprised of ammonium sulfate [*Srivastava et al.*, 1997], while $\beta_{9.11}/\beta_{10.59}$ for partially ammoniated aerosol (consisting of a mixture of ammonium sulfate, sulfuric acid, and dust) has a range of 2-10. However, using infrared wavelengths to compute infrared β ratios poses a problem because large refractive index variations can occur over these wavelengths [*Kent et al.*, 1983], leading to results which can be ambiguous. Note that since $\beta_{0.53}/\beta_{1.06}$ are small these data do not provide information on chemical composition.

5.1. Japan

The dominant vertical aerosol feature (section 4.1) present during the flight near Japan will be examined for aerosol composition using CN time series data, LOPC-modeled β, 9.11- and 10.59-μm β, and corresponding backscatter ratio for the whole flight (Figure 10). For flight levels above 8.5-km the infrared β was generally below 10^{-10} m^{-1} sr^{-1}. A low CN refractory component (Figure 10c) implied that sulfuric acid dominated the small-particle regime (<0.1-μm diameter). Best agreement between the LOPC-modeled and lidar-measured β data was found using sulfuric acid composition to compute the LOPC-modeled β. The few $\beta_{9.11}/\beta_{10.59}$ data above 8.5 km (Figure 10d) indicate a ratio around 2, which is also consistent with sulfuric acid particles in a low β regime [*Srivastava et al.*, 1995]. A moderate agreement is noted between the CW lidar and FSSP-modeled β at the 11.5-km level, which is also indicated by the good agreement between the average value data (Figure 6). Since β at this altitude was due to moderate concentrations of sulfuric acid particles with upper diameter limit below 1 μm, the FSSP count statistics are adequate to estimate β from these size distributions. At flight levels below 8 km the aerosol composition contained a much larger refractory CN component (Figure 10c). Both the measured and modeled β were greater than $\sim 10^{-8}$ m^{-1} sr^{-1}, with $\beta_{9.11}/\beta_{10.59}$ remaining less than two. This indicates a composition dominated by sea salt and/or dust-type aerosol [*Srivastava et al.*, 1995]. However, Plate 1 indicates a plume of aerosol extending upward from the MBL to ~8.5 km that is expected to be composed predominantly of sea salt. FSSP- and LOPC-modeled and CW lidar-measured β all show a dip at the beginning of the 6.5-km flight level. This indicates that a region was encountered with more volatile particles, most likely composed of sulfuric acid since $\beta_{9.11}/\beta_{10.59}$ remains below two. The large drop in nonrefractory CN at 3.5 km just after 0500 UTC appears to be correlated with an order of magnitude change in β as measured by the CW lidar. This indicates a change in composition, where sea salt or other refractory material may have been partially replaced by a volatile aerosol. The CW β and the JPL colorized β image (not shown) at 3.5 km showed a cleaner region where β in each case was an order of magnitude lower. Since the total CN concentration increased, the change must be due to an increase in small sulfuric acid particles, as $\beta_{9.11}/\beta_{10.59}$ remained below two. It is noted that the FSSP-modeled β (near 0500 UTC in Figure 10b) did not respond nearly as strongly to these changes. At 8.5-km, β returned to values below 10^{-10} m^{-1} sr^{-1}, and $\beta_{9.11}/\beta_{10.59}$ exhibited a greater range of fluctuation (<2 - ~3.5).

An interesting feature was noted in the β plots shown in Figure 10b, over the periods 0315-0400 UTC and 0615-0700 UTC at 9.8 and 8.5 km, respectively. During these periods the 300-s CW lidar $\beta_{9.11}$ showed only small fluctuations about a mean value. Likewise, the JPL lidar $\beta_{9.25}$, averaged 1 to 2 km from the aircraft, exhibited a similar behavior. However, the 300-s FSSP- and much longer averaged LOPC-modeled β data show large variations over these two periods. It is noted that since the FSSP-modeled β is below 10^{-10} m^{-1} sr^{-1}, it could be up to a factor of 3 too low [*Cutten et al.*, 1996] than the measured β, because of inadequate count statistics. This feature was also observed at the 12.6-km flight level in the Hawaii flight and in several of the other GLOBE transit flights, all in the infrared β range of 10^{-10}-10^{-11} m^{-1} sr^{-1}. Furthermore, a significant variation occurred in the refractory CN over the 0615-0700 UTC period which is correlated with the FSSP-modeled β variation. The $\beta_{9.11}/\beta_{10.59}$ plot (Figure 10d) exhibits variation over this period but is poorly correlated with FSSP-modeled β. The near-steady CW lidar β at both wavelengths is a result of their much larger sampling volumes. The lidars are sampling many more large particles (>1 μm) which contribute to a significant fraction of the β compared with the much smaller sample volume of the OPCs. If the composition of these large particles was constant over the period, then little variation would result in the lidar β. On the other hand, variations seen in the OPC data are probably due to sampling aerosols <1-μm diameter whose composition varied along the flight path. For example, during the 0615-0700 UTC period, a small sulfuric acid aerosol component was initially encountered, which changed to a sulfuric acid-dust mixture that left a nonvolatile component after heating and which finally reverted to mostly sulfuric acid.

The analysis for the Japan flight has revealed two interesting features. First, the aerosol plume, evident in the 1.06-μm colorized β plot (Plate 1), contained predominantly MBL sea

Table 2. Calculated Backscatter Coefficient Ratios for Several Wavelength Pairs, Aerosol Compositions, and Geometric Mean Radius (r_g) Values

	r_g, μm	Sea Salt	Dust	Ammonium Sulfate	Sulfuric Acid
$\beta_{0.53}/\beta_{1.06}$	0.15	–	2.5	3.5	2.5
	0.6	2	2	2.5	2
$\beta_{1.06}/\beta_{9.25}$	0.15	–	225	20	65
	0.6	25	5	2.5	5
$\beta_{9.11}/\beta_{10.59}$	0.15	–	2	13	2.5
	0.6	2-3	2	10	1.5

N_o = 1 particle cm^{-3} and σ_g = 1.5 were assumed.

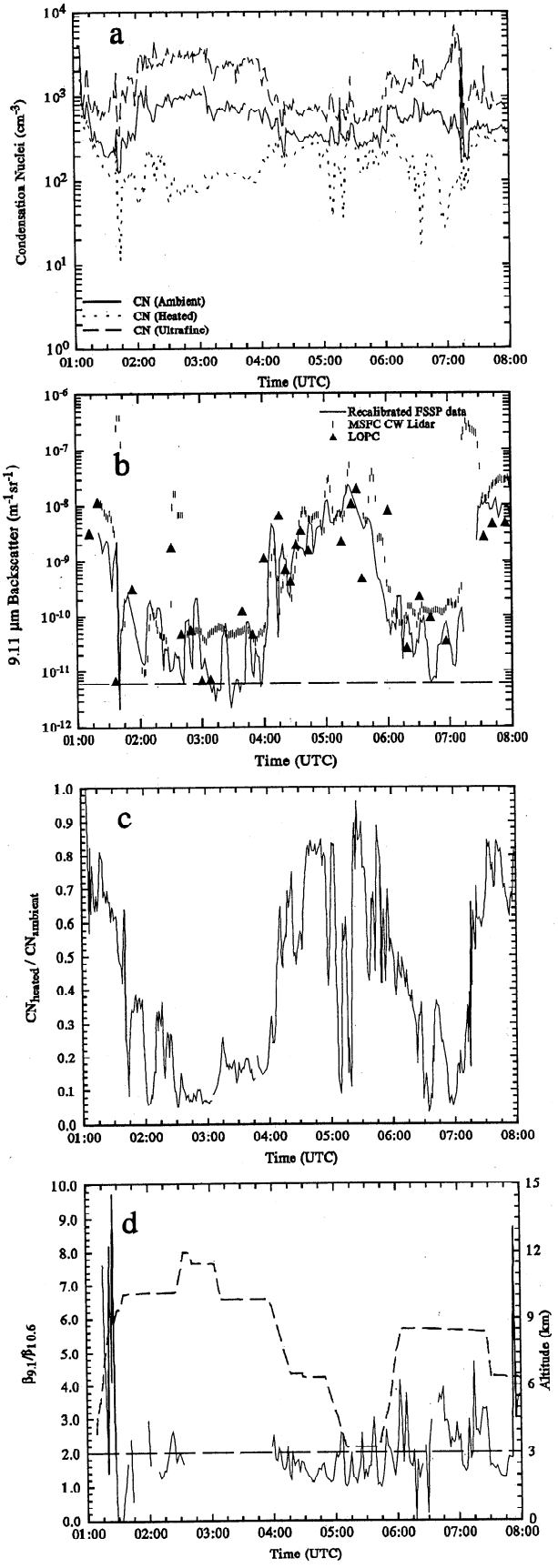

Figure 10. Flight level measurements of (a) condensation nuclei concentration, (b) measured and modeled 9.11-μm aerosol backscatter (horizontal line represents CW lidar sensitivity level), (c) refractory condensation nuclei concentration, and (d) ratio of $\beta_{9.11}/\beta_{10.59}$ aerosol backscatter, for entire flight near Japan.

salt aerosol which had risen to ~8.5 km. The lower CN concentrations (Figure 10a) at 3.2- and 6.5-km flight levels below 8 km indicate the presence of an aerosol predominantly from the MBL. The aerosol plume may have also contained sulfuric acid particles (<1-μm diameter) that originated from pollution sources in Japan. One layer observed at 3.5 km was probably the result of concentrations of pollution-type particles. Above the aerosol plume (~9 km) all measured and modeled β data, as well as β ratio data, indicate a free tropospheric sulfuric acid aerosol which is normally found at these altitudes. Second, it was found that in certain aerosol regimes, both of the in-flight OPC sensors showed a widely varying, modeled $\beta_{9.25}$, while the lidar-measured $\beta_{9.25}$ showed minimal variation. This can be explained if the large particles (>2-μm diameter), which the lidars would sample adequately, did not change composition and the smaller particles did. Thus a coarse form of composition segregation occurred when using sensors with very small and very large sampling volumes to infer β values. This augments the point that a fully representative infrared β whose real value is $<10^{-10}$ m^{-1} sr^{-1} can only be obtained if the sensor with a large sampling volume is used [*Cutten et al.*, 1996].

5.2. Hawaii

The microphysics analysis was restricted because of less comprehensive coverage of the lidar data compared with the Japan flight. However, OPC-derived β data combined with one ratio ($\beta_{1.06}/\beta_{9.25}$) profile (Figure 8) provide some insight into the aerosol microphysics prevailing at the time in the lower altitudes. It should be noted the two averaged $\beta_{1.06}$ profiles in Figure 8 (one over 40 min, the other over 10 min) compared very well below 5 km, indicating the longer averaging period encompassing all three legs did not produce significant differences from the first leg of the flight. The nadir $\beta_{1.06}/\beta_{9.25}$ profile shows values ranging from 25 to about 110 where the lower $\beta_{1.06}/\beta_{9.25}$ values correspond to a wavelength dependence exponent of ~1.5, implying the presence of large dust and/or ammoniated particles over the altitude range 3.6-4.1 km. In addition, the CN data measured at 4-km flight level between 2200 and 2300 UTC indicate that a strong refractory component was present for this size range. In Figure 9 LOPC-modeled $\beta_{9.11}$ showed best agreement with CW lidar $\beta_{9.11}$ using a composite aerosol mixture based on modeling by *Srivastava et al.* [1997] which was modified with a hygroscopic refractory component representative of, for example, sulfuric acid coated dust. LOPC- derived $\beta_{1.06}$ were slightly higher than the FSSP-modeled $\beta_{1.06}$ for the same modeled composition. It is noted that when the hygroscopic dust component was replaced with a nonhygroscopic dust, the calculations yield a noticeably lower LOPC-modeled $\beta_{9.11}$. At 2-km altitude the β ratio curve (Figure 8) indicates a decrease in the concentration of large aerosol particles with height and a possible change in composition to a partially ammoniated aerosol; there is only a small decrease in $\beta_{1.06}$. It should be noted that spatial resolution of the data is not a factor, since vertical resolution of the GSFC lidar is half that of JPL lidar. The wavelength exponent for aerosol β in this layer is around 2.2. Below 2 km the ratio fluctuates around a value of about 55 (wavelength exponent of ~1.95), where both $\beta_{1.06}$ and $\beta_{9.25}$ are high. In this case it would appear that a refractory material again was responsible for the high β. Thus, from near the surface to 5 km, there is a change in large particle numbers and/or particle composition; this behavior may have been caused by aerosol plume emanating from volcanic activity that was occurring at that time on the big island of Hawaii.

6. Conclusions

The main conclusion from the intercomparison is that all measured and modeled β data showed reasonable agreement at moderate β levels but lesser agreement in low β conditions which often occur in the middle and upper troposphere. In the latter case the pulsed lidar data showed the largest disagreement with the flight level sensor data, whereas differences within the in-flight sensor data were generally smaller. This significant difference in β between the OPCs and pulsed lidars may be due to the large differences in sample volumes, the sampling volume factor being as much as 10^8 between the pulsed lidars and the FSSP sensor. Thus the lidar β will be more representative for both wavelength regions because (1) the lidars sample the larger particles (which contribute most to β for the 9.25-μm region) more frequently, and (2) there is no comparable cutoff in the submicrometer particle size range (which the OPCs exhibit) that affect the 1.06-μm region. Limited data from the upper tropospheric region did not indicate that the FSSP-modeled infrared β was underestimated when $\beta < 10^{-10}$ m^{-1} sr^{-1} [*Cutten et al.*, 1996].

This study has also revealed that a suite of airborne instruments, like the one described here, can provide detailed information on the prevailing aerosol. The two distinct aerosol regimes identified in the Japan flight, along with smaller changes within these regimes, attest to this. Using lidar β ratio data for several wavelength pairs can reduce the ambiguity in determining aerosol size ranges responsible for β at a particular wavelength. Furthermore, β ratios, when combined with theoretical calculations using aerosol constituents commonly found in the tropospheric aerosol, can allow further information to be retrieved remotely about the composition [*Srivastava et al.*, 1997].

Finally, this study has highlighted the usefulness of correlating data from measured β ratios with CN refractory and nonrefractory particle numbers to derive the aerosol composition. It also provided evidence that aerosol chemical composition can be segregated based on sample volume size. Large lidar sample volumes can sample large particles much more efficiently; when the particle composition differs from that of smaller particles, the lidar measurements can give a different β from that modeled using the OPC size distributions.

Acknowledgments. The authors gratefully acknowledge Eugene McCaul Jr. for providing the meteorological summaries for the GLOBE flights and David Tratt, Sury Chudamani, and Diana Chambers for providing the JPL, GSFC, and MSFC lidar data, respectively. The authors also gratefully acknowledge Ramesh Kakar, Office of Mission to Planet Earth, NASA Headquarters, without whose support this work would not have been possible. This work was supported under NASA cooperative agreement NCC8-22 and preceding contracts since 1990.

References

Albrecht, B. A., Aerosols, cloud microphysics, and fractional cloudiness, *Science, 245*, 1227-1230, 1989.

Bowdle, D. A., J. Rothermel, J. E. Arnold, and S. F. Williams, The Global Backscatter Experiment (GLOBE) Pacific survey mission, results and implications for LAWS, in *Proceedings of the Coherent Laser Radar: Technology and Applications Topical Meeting*, pp. 290-292, Optical Society of America, Washington, D.C., 1991.

Charlson, R. J., S. E. Schwartz, J. M. Hales, R. D. Cess, J. A. Coakley Jr., J. E. Hansen, and D. J. Hofmann, Climate forcing by anthropogenic aerosols, *Science*, *255*, 423-430, 1992.

Clarke, A. D., A thermo-optic technique for in situ analysis of size-resolved aerosol physicochemistry, *Atmos. Environ., 25A*, 635-644, 1991.

Clarke, A. D., Atmospheric nuclei in the Pacific midtroposphere: Their nature, concentration, and evolution, *J. Geophys. Res., 98*, 20,633-20,647, 1993.

Coakley, J. A., and R. D. Cess, Response of the NCAR community climate model to the radiative forcing of naturally occurring tropospheric aerosol, *J. Atmos. Sci., 42*, 1677-1692, 1985.

Cutten, D. R., R. F. Pueschel, V. Srivastava, D. A. Bowdle, A. D. Clarke, J. Rothermel, J. D. Spinhirne, and R. T. Menzies, Multiwavelength comparison of modeled and measured remote tropospheric aerosol backscatter over Pacific Ocean, *J. Geophys. Res., 101*, 9375-9389, 1996.

Kent, G. S., G. K. Yue, U. O. Farrukh, and A. Deepak, Modeling atmospheric aerosol backscatter at CO_2 wavelengths, 1, Aerosol properties, modeling techniques and associated problems, *Appl. Opt., 22*, 1655-1665, 1983.

Menzies, R. T., and D. M. Tratt, Airborne CO_2 coherent lidar for measurements of atmospheric aerosol and cloud backscatter, *Appl. Opt., 33*, 5698-5711, 1994.

Pueschel, R. F., J. M. Livingston, G. V. Ferry, and T. E. DeFelice, Aerosol abundances and optical characteristics in the Pacific basin free troposphere, *Atmos. Environ., 28*, 951-960, 1994.

Rothermel, J., D. M. Chambers, M. A. Jarzembski, V. Srivastava, D. A. Bowdle, and W. D. Jones, Signal processing and calibration of continuous wave focused CO_2 Doppler lidars for atmospheric backscatter measurement, *Appl. Opt., 35*, 2083-2095, 1996.

Spinhirne, J. D., S. Chudamani, J. F. Cavanaugh, and J. L. Bufton., Aerosol and cloud backscatter at 1.06, 1.54, and 0.53 μm by airborne hard-target-calibrated Nd:YAG/methane Raman lidar, *Appl. Opt., 36*, 3475-3490, 1997.

Srivastava, V., M. A. Jarzembski, and D. A. Bowdle, Comparison of calculated aerosol backscatter at 9.1 and 2.1 μm wavelengths, *Appl. Opt., 31*, 1904-1906, 1992.

Srivastava, V., D. A. Bowdle, M. A. Jarzembski, J. Rothermel, D. M. Chambers, and D. R. Cutten, High-resolution remote sensing of atmospheric sulfate aerosols from CO_2 lidar, backscatter, *Geophys. Res. Lett., 22*, 2373-2376, 1995.

Srivastava, V., A. D. Clarke, M. A. Jarzembski, and J. Rothermel, Comparison of modeled backscatter using measured aerosol microphysics with focused CW lidar data over the Pacific, *J. Geophys. Res., 102*, 16,605-16,617, 1997.

D. A. Bowdle and D. R. Cutten, Earth System Science Laboratory, Global Hydrology and Climate Center, University of Alabama in Huntsville, Huntsville, AL 35899. (e-mail: David.Bowdle@msfc.nasa.gov; Dean.Cutten@msfc.nasa.gov)

A. D. Clarke, School of Oceanography, University of Hawaii, Honolulu, HI 96822. (e-mail: tclarke@soest.hawaii.edu)

R. T. Menzies, NASA Jet Propulsion Laboratory, Pasadena, CA 91109. (e-mail: Robert.Menzies@jpl.nasa.gov)

R. F. Pueschel, NASA Ames Research Center, Moffett Field, CA 94035. (e-mail: rpueschel@mail.arc.nasa.gov)

J. Rothermel, Global Hydrology and Climate Center, NASA Marshall Space Flight Center, Huntsville, AL 35806. (e-mail: Jeffry.Rothermel @msfc.nasa.gov)

J. D. Spinhirne, NASA Goddard Space Flight Center, Greenbelt, MD 20771. (e-mail: jspin@virl.gsfc.nasa.gov)

V. Srivastava, Universities Space Research Association, Global Hydrology and Climate Center, Huntsville, AL 35806. (e-mail: Vandana.Srivastava@msfc.nasa.gov)

(Received July 21, 1997; revised January 20, 1998; accepted March 18, 1998.)